



**HAL**  
open science

# Heterogeneous Enantioselective Catalysis with Chiral Encoded Mesoporous Pt-Ir Films Supported on Ni Foam

Sunpet Assavapanumat, Sapon Butcha, Somlak Ittisanronnachai, Alexander Kuhn, Chularat Wattanakit

► **To cite this version:**

Sunpet Assavapanumat, Sapon Butcha, Somlak Ittisanronnachai, Alexander Kuhn, Chularat Wattanakit. Heterogeneous Enantioselective Catalysis with Chiral Encoded Mesoporous Pt-Ir Films Supported on Ni Foam. Chemistry - An Asian Journal, 2021, 16 (21), pp.3345-3353. 10.1002/asia.202100966 . hal-03516170

**HAL Id: hal-03516170**

**<https://cnrs.hal.science/hal-03516170>**

Submitted on 7 Jan 2022

**HAL** is a multi-disciplinary open access archive for the deposit and dissemination of scientific research documents, whether they are published or not. The documents may come from teaching and research institutions in France or abroad, or from public or private research centers.

L'archive ouverte pluridisciplinaire **HAL**, est destinée au dépôt et à la diffusion de documents scientifiques de niveau recherche, publiés ou non, émanant des établissements d'enseignement et de recherche français ou étrangers, des laboratoires publics ou privés.

# Heterogeneous Enantioselective Catalysis with Chiral Encoded Mesoporous Pt-Ir Films Supported on Ni Foam

Sunpet Assavapanumat,[a] Sapon Butcha,[a,b] Somlak Ittisanronnachai,[a] Alexander Kuhn,[a,b] Chularat Wattanakit\*,[a]

[a] S. Assavapanumat, S. Butcha, S. Ittisanronnachai, A. Kuhn, C. Wattanakit

School of Energy Science and Engineering, School of Molecular Science and Engineering, Frontier Research Center (FRC), and Nanocatalysts and Nanomaterials for Sustainable Energy and Environment Research Network of NANOTEC

Vidyasirimedhi Institute of Science and Technology (VISTEC)

Rayong, Thailand

E-mail: chularat.w@vistec.ac.th

[b] S. Butcha, A. Kuhn

University of Bordeaux, CNRS, UMR 5255, Bordeaux INP, Site ENSCBP, 16 avenue Pey Berland, 33607, Pessac, France

Supporting information for this article is given via a link at the end of the document.

**Abstract:** The development of heterogeneous catalysts for asymmetric synthesis is one of the most challenging topics in chemistry, as it allows obtaining enantiomerically pure compounds. Recently, metal layers incorporating molecular chiral cavities, obtained by electroreduction of a metal source in the simultaneous presence of a non-ionic surfactant and asymmetric molecules, have been proposed for a wide range of applications, including enantioselective electroanalysis and electrosynthesis, as well as chiral separation. In contrast to this previous work, solely based on electrochemical phenomena, herein we designed and employed nanostructured chiral encoded Pt-Ir alloys, supported on high surface area nickel foams, as heterogeneous catalysts for the asymmetric hydrogenation of aromatic ketones. Fine-tuning the experimental conditions allows achieving very high enantioselectivity (> 80 %), combined with improved catalyst stability.

## Introduction

Rational engineering of chiral surfaces is of crucial importance in heterogeneous catalysis in order to get access to enantiomerically pure compounds (EPCs), which have important applications in various fields, ranging from academic topics<sup>1</sup> to the commercial synthesis of agrochemicals and pharmaceuticals<sup>2</sup>. Although many chiral materials are based on organic polymers and semiconductors<sup>3</sup>, there are also numerous examples of metal surfaces bearing chiral surface features<sup>4</sup>. For instance, Ag surfaces with a high Miller index have been obtained by precision cutting, revealing surfaces such as Ag(643)R and Ag(643)S, being non-superimposable mirror images of each other<sup>7</sup>. However, such surfaces sometimes suffer also from drawbacks such as a complicated preparation process, limited enantiodiscrimination properties due to a small number of active sites, and low stability<sup>5</sup>.

High enantioselectivity is however observed for enzymatic catalysts, able to generate a certain type of chiral products under mild conditions<sup>6</sup>. Nonetheless, poor stability, low efficiency under industrial conditions and unspecific adsorption of molecules at the active site are considered as the unavoidable limitations in the frame of their use for organic synthesis<sup>7</sup>. In order to mimic biocatalysts with inorganic materials, several approaches have been intensively studied for breaking the symmetry at metal surfaces, e.g. adsorption of chiral entities on metal surfaces<sup>8</sup>, chiral molecular grafting of metal surfaces<sup>9</sup>, cutting surfaces to generate a high Miller index plane<sup>10</sup>, and chiral imprinting of metal surfaces<sup>4b,11</sup>. Among them, chiral encoded metals obtained by a molecular imprinting approach are promising materials to retain chiral information, even after removal of the chiral templates<sup>4b,11</sup>.

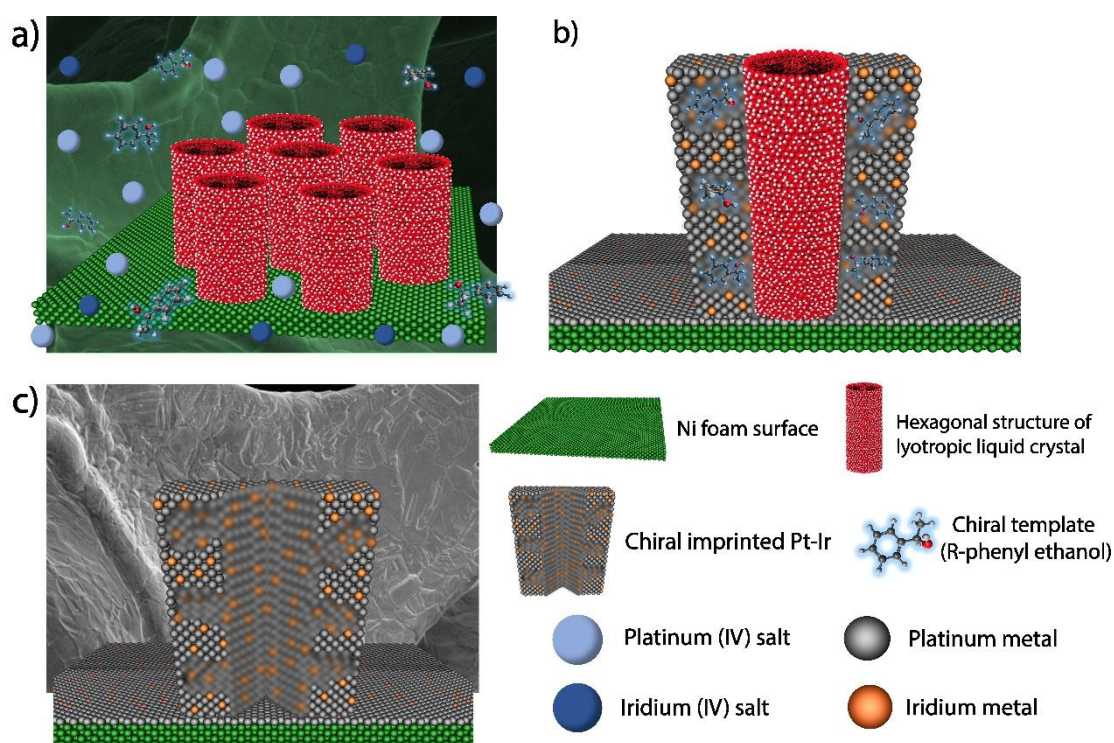
It is worth mentioning that chiral metal surfaces combined with mesoporous structures reveal outstanding properties, in particular a significant increase in active surface area, with enhanced chiral recognition properties<sup>12</sup>. Recently, highly ordered mesoporous structures with chiral features have been reported as a new class of materials, namely Chiral Imprinted Mesoporous Metals (CIMMs). They are obtained by electrodeposition of metal in the simultaneous presence of a self-assembled supramolecular template structure, composed of a hexagonal lyotropic liquid crystal phase and chiral molecules, acting as mesoporegens and chiral templates, respectively<sup>4b</sup>. Apart from analytical applications<sup>4b,11b</sup>, these metal surfaces have been used for various potential applications, ranging from chiral separation<sup>13</sup> and enantioselective actuation<sup>11d</sup> to asymmetric electrosynthesis<sup>14</sup>. Concerning the latter aspect, CIMMs have been employed as working electrodes, yielding initially an only moderate enantiomeric excess (%ee) <sup>14a</sup>. However, by fine-tuning the conditions of the electroreduction, a very high %ee (>95%) could be achieved, especially when using a pulsed electrosynthesis strategy with imprinted bimetallic Pt-Ir alloys as electrode material<sup>14b-14d</sup>.

While chiral electrosynthesis is a less common approach, conventional asymmetric synthesis is a much more wide-spread option to obtain EPCs, in particular when using a heterogeneous catalyst with chiral surface properties, which can be easily recovered after the catalytic reaction. Typically, chiral heterogeneous metal catalysts have been obtained by one of the following approaches: (i) chiral surface grafting<sup>15</sup>; (ii) chiral ligand-modified metal nanoparticles<sup>16</sup>; (iii) molecular imprinting of metal surfaces<sup>17</sup>; (iv) entrapment of chiral compounds inside metal particles<sup>18</sup>. Among these strategies, molecular imprinting and entrapment of chiral molecules in metal layers are interesting concepts to establish chiral information on solid surfaces, due to their versatility in terms of the types of imprinted molecules and the available solid matrices, comprising noble and non-noble metals<sup>18,19</sup>.

In the present study, we demonstrate that a chiral imprinted mesoporous bimetallic Pt-Ir alloy supported on Ni foam can be advantageously used as heterogeneous catalyst for asymmetric synthesis of a chiral compound via hydrogenation of an aromatic ketone. The alloy has been successfully prepared by co-electroreduction of Pt and Ir in the simultaneous presence of a non-ionic surfactant (Brij C10) and molecular chiral templates. Subsequently, in order to verify the presence of chiral information imprinted on the alloy surface, the enantioselective discrimination between the two stereoisomers of a chiral molecule (Phenylethanol, PE) has been tested by Differential pulse voltammetry (DPV). Finally, when using this material as heterogeneous catalyst in the presence of the prochiral precursor (Acetophenone, ACE) and hydrogen, a fine-tuning of the conditions of catalysis, in particular by using a pulsed synthesis process, allows achieving high enantioselectivity (up to 85 %ee).

Results and Discussion

Catalytic hydrogenation of aromatic ketones can be performed, among others, with platinum black in a hydrogen atmosphere. For examples the hydrogenation of ACE is possible with high conversion efficiency and selectivity for PE<sub>20</sub>. However, the uncontrolled stereochemistry results in a racemic mixture of R-phenylethanol (RPE) and S-phenylethanol (SPE). Typically, to obtain more or less enantiopure PE products, different metals have been widely used as catalysts for asymmetric hydrogenation<sup>21</sup>. Recently, enantioselective synthesis of PE via hydrogenation of ACE has been achieved by its electroreduction on electrocatalysts having the appropriate handedness, including noble metals (Pt), non-noble metals (Ni), and bimetallic alloys (Pt-Ir)<sup>4b,6c,13-14</sup>. The latter showed higher enantioselectivity and catalyst stability compared to the corresponding monometallic electrocatalyst. However, modifying planar surfaces with these catalyst structures leads to a restricted accessibility of the active chiral sites by the reactants due to diffusion limitations, eventually resulting in a lower catalytic performance. In order to circumvent these limitations, deposition of the catalytically active layer on a support with high surface area is a promising strategy. Nickel (Ni) foam was used in this work as a solid support to improve the diffusion of guest molecules. The chiral imprinted mesoporous Pt-Ir, supported on Ni foam, has been prepared by electrodeposition in the simultaneous presence of metal precursors, a self-assembled lyotropic liquid crystal, and the desired amount of chiral template as illustrated in Scheme 1. PE has been chosen as a molecular template to introduce specific chiral sites inside the mesoporous structure. The presence of a hydroxy group in PE and also as a head group of polyoxyethylene (10) cetyl ether (Brij C10), allows the formation of a well-defined hexagonal liquid crystal phase (H1) interacting with the chiral template by hydrogen-bonding. Scheme 1a illustrates the self-assembled chiral plating gel on Ni foam before electrodeposition. The bimetallic alloy is subsequently electrodeposited throughout the template structure by controlling the injected charge density (Scheme 1b). The final chiral imprinted mesoporous Pt-Ir on Ni foam is obtained after removal of the chiral template and surfactant as shown in Scheme 1c.



Scheme 1. Illustration of the synthesis of a chiral encoded mesoporous bimetallic Pt-Ir alloy supported on Ni foam: a) formation of the lyotropic liquid crystalline phase in the presence of metal salt and chiral molecules on Ni foam; b) electrodeposition through the self-assembled template structure; c) Final chiral imprinted mesoporous Pt-Ir alloy supported on Ni foam after template removal.

The surface morphology of the initial 3D Ni foam has been investigated by scanning electron microscopy (SEM) with low and high magnification as can be seen in Figure S1. The Ni foam surface is homogeneous and smooth, and its composition was confirmed by EDS elemental mapping. The structure, morphology, and elemental composition of as-synthesized chiral imprinted Pt-Ir on Ni foam obtained by using a charge density of  $8 \text{ C cm}^{-2}$  is illustrated in Figure S2 and S3. After electrodeposition of chiral encoded Pt-Ir, a darker homogeneous thin film covers the Ni foam (Figure 1a and 1b). The thickness of the film can be easily adjusted by varying the deposition charge density. For examples the layer is 145.0, 297.3, and 458.4 nm thick when using deposition charge densities of 4, 8, and  $12 \text{ C cm}^{-2}$ , respectively (Figure S2 and Table S1). Moreover, the macroscopic surface structure at the junction between the bare Ni surface and the bimetallic layer is illustrated in Figure 1e (inset), and EDS mapping was carried out to investigate the elemental distribution at this junction (Figure 1f-h and Figure S3), revealing that Pt and Ir are evenly distributed.

To verify the mesoporous structure of the catalytic layer, HR-TEM images have been recorded and reveal a highly ordered hexagonal mesoporous structure with a pore size of  $6.52 \pm 0.35 \text{ nm}$  (Figure 2a and 2b) for a sample generated with a charge density of  $8 \text{ C cm}^{-2}$ . In addition, the alloy character has been investigated with X-ray diffraction (Figure S4). The XRD profile confirms the presence of the three main components, Pt, Ir and Ni. It clearly shows high intensity peaks at  $2\theta$  of  $44.5^\circ$  and  $52.0^\circ$ , corresponding to the Miller Indices (111) and (200) of nickel (Figure S4a).<sup>22</sup> The characteristic XRD pattern of Pt in the alloy appears at  $2\theta$  of  $40.0^\circ$  and  $46.5^\circ$  (Figure S4b) originating from its (111) and (200) planes, respectively. The values are shifted to slightly higher  $2\theta$  angles compared to a pure Pt

film on Ni foam due to the presence of Ir. <sup>14d,23</sup> Although the characteristic Ir peak cannot be seen directly in the case of the Pt-Ir sample, due to the very low amount of Ir with respect to Pt (10 % of Ir see Table S2), the slight shift of the Pt peak can be attributed to a partial substitution of Pt by Ir, which is consistent with previous studies.<sup>14d</sup> The composition and alloy structure of the chiral imprinted Pt-Ir film has also been studied by X-ray photoelectron spectroscopy (XPS) in comparison to monometallic Pt, deposited on nickel foam. The XPS spectra of Pt and Ir in monometallic as well as bimetallic layers obtained by using various deposition charge densities are shown in Figure 2c and 2d. The binding energies of 69.7 eV and 73.1 eV for Pt 4f<sub>7/2</sub> and 58.8 eV and 61.8eV for Ir 4f<sub>7/2</sub> are consistent with the standard cards of these elements.<sup>14d,23-24</sup> Remarkably, the characteristic peaks of Pt and Ir of the bimetallic Pt-Ir samples are slightly shifted to a higher binding energy due to the charge transfer between Pt and Ir.<sup>25</sup> Obviously the Ir signal is more affected, because it is embedded in a majority of Pt atoms and therefore shifts are more pronounced compared to Pt, which is the major component of the matrix and therefore its signal is less disturbed by the small fraction of Ir. The relative amount of Pt and Ir in the alloy was confirmed by inductively coupled plasma optical emission spectroscopy (ICP-OES), and values of 90% and 10% have been found, respectively (Figure S5 and Table S2). In order to measure the active surface area of the bimetallic Pt-Ir films prepared with various deposition charge densities, cyclic voltammograms (CV) in 0.5 M H<sub>2</sub>SO<sub>4</sub> in the potential range from -0.25 to 1.25 V vs Ag/AgCl are shown in Figure 3a. The characteristic peaks between -0.25 and 0.20 V relate to proton adsorption and desorption (hydrogen region) on Pt surfaces, while the characteristic oxidation of the Pt surface and reduction of PtO<sub>n</sub> appear at 0.80 and 0.45 V, respectively.<sup>24b</sup> Fortunately, there is only little interference of oxidation currents originating from the Ni foam used as a support, as shown in Figure S6. It allows us observing the electroactive surface area of the Pt-Ir alloy in the hydrogen adsorption and desorption regions without the interference of Ni characteristics. The electroactive surface area of the prepared Pt-Ir films is significantly increasing as a function of deposited charge density with 341, 826, 1680, and 2560 cm<sup>2</sup> for those synthesized with 4, 6, 8 and 12 C cm<sup>-2</sup>, respectively, as can be seen in Figure 3b.

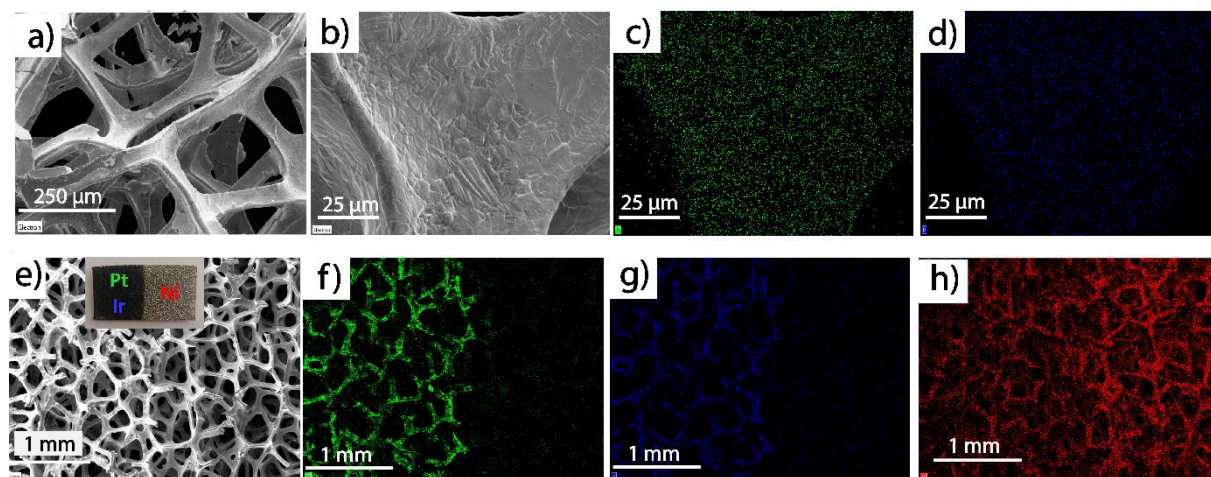


Figure 1. Surface morphology characterization of a chiral imprinted mesoporous Pt-Ir film supported on Ni foam: a) and b) SEM images of chiral encoded Pt-Ir deposited on Ni foam; and c) and d) EDS mapping of Pt (green) and Ir (blue). The bottom panels demonstrate the surface morphology at the

junction between pristine Ni foam and the part covered with Pt-Ir. e) SEM images and f), g) and h) EDS mapping of Pt (green), Ir (blue) and Ni (red), respectively.

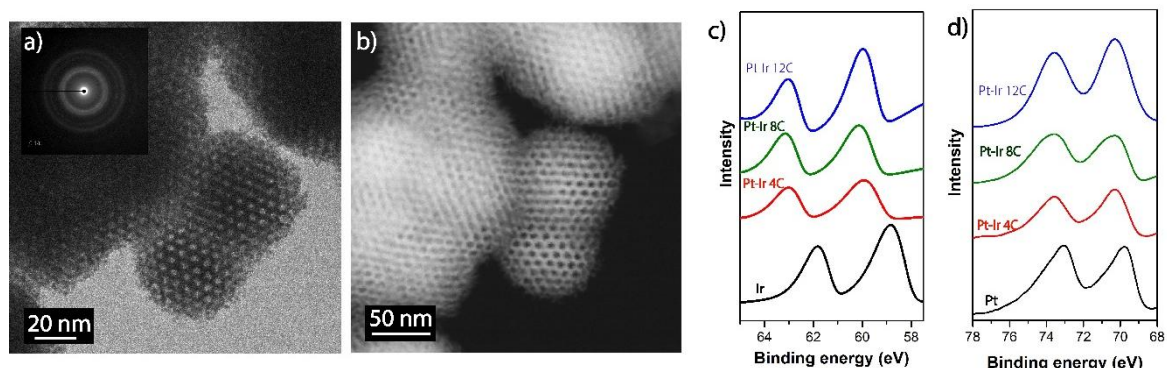


Figure 2. Mesoporous structure and alloy structure confirmation: a) TEM image of a chiral imprinted Pt-Ir film revealing the well-ordered hexagonal mesopores (scale bar 20 nm); b) HR-TEM image of bimetallic film (scale car of 50 nm). c) XPS spectra in the Ir binding energy region of standard Ir on Ni foam (black) and of RPE imprinted bimetallic Pt-Ir on Ni foam when using deposition charge densities of 4 C cm<sup>-2</sup> (red), 8 C cm<sup>-2</sup> (green), and 12 C cm<sup>-2</sup> (blue); d) XPS spectra in the Pt binding energy region of standard Pt on Ni foam (black) and the bimetallic Pt-Ir on Ni foam when using deposition charge densities of 4 C cm<sup>-2</sup> (red), 8 C cm<sup>-2</sup> (green) and 12 C cm<sup>-2</sup> (blue).

Before performing catalytic hydrogenation with the synthesized materials, it is necessary to verify its enantioselective recognition abilities. Differential Pulse Voltammograms (DPV) in the potential range from 0.3 to 0.8 V versus Ag/AgCl were recorded with the foam supported alloy in solutions containing the 3,4-dihydroxyphenylalanine (DOPA) enantiomers. The oxidation signals show different intensities as a function of the imprinted PE enantiomer (Figure 3c and 3d). RPE encoded electrodes preferentially react with D-DOPA, whereas SPE imprinted surfaces have a higher affinity for L-DOPA, clearly indicating the

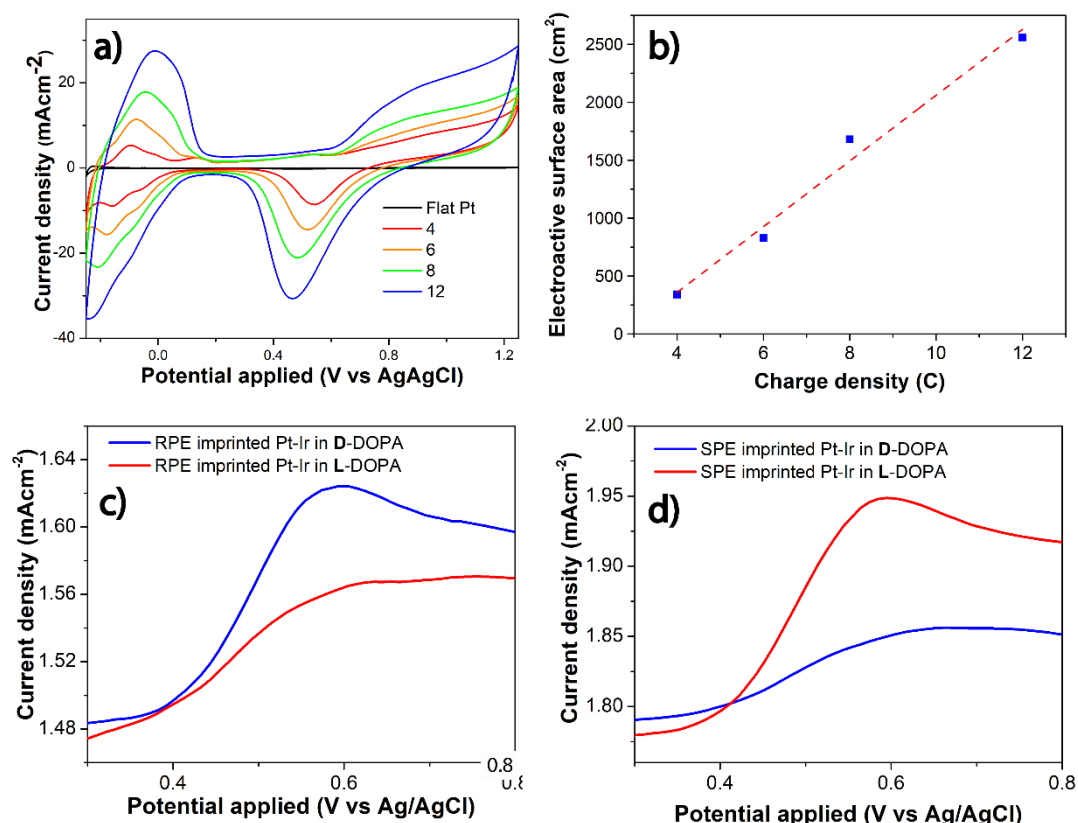


Figure 3. Electrochemical characterization of the chiral encoded bimetallic Pt-Ir alloy on Ni foam. a) Cyclic voltammograms of the alloy obtained using various deposition charge densities compared to the flat Pt in 0.5 M H<sub>2</sub>SO<sub>4</sub> at a scan rate of 100 mVs<sup>-1</sup>, b) Linear relationship between electroactive surface area and deposition charge density, c) Differential Pulse Voltammogram (DPV) of chiral Pt-Ir imprinted with RPE in 4 mM D-DOPA (blue) and L-DOPA (red) in 50 mM HCl as a supporting electrolyte, d) DPV of the chiral Pt-Ir imprinted with SPE in 4 mM D-DOPA (blue) and L-DOPA (red) in 50 mM HCl.

presence of chiral features in the alloy matrix. In order to exclude artefacts due to presence of chiral template molecules, left over from the imprinting process, the template removal was followed by UV-Vis spectroscopy prior to the enantioselective recognition studies. As shown in Figure. S7, the absorbance of a series of washing solutions was recorded as a function of rinsing time. The absorbance signal of PE ( $\lambda_{max}$ = 250 nm) in the first rinsing solution is rather high, meaning that a lot of chiral templates is leaving the metal matrix. However, after several consecutive washing cycles, the amplitude of this characteristic peak dramatically decreases. In particular, no more chiral molecules can be detected in the rinsing solution after washing for 30 h.<sup>14b-14d</sup> It is noteworthy that even when using one type of chiral molecule (PE) for generating the recognition sites, it allows the stereoselective discrimination of another type of chiral molecule (DOPA) if they have similar stereocentre configurations<sup>11b</sup>. To further validate the different amplitudes measured for the chiral recognition experiment, a control experiment has been carried out after erasing the chiral information by applying a very aggressive positive potential to oxidize the alloy<sup>14d</sup>. As expected, identical amplitudes for L-DOPA and D-DOPA oxidation are measured for both electrodes after

exposing them to very positive potentials in a “cleaning cycle” from -0.25 to 1.80 V versus Ag/AgCl (Figure S8a), very similar to what is obtained for a non-imprinted electrode (Figure S8b).

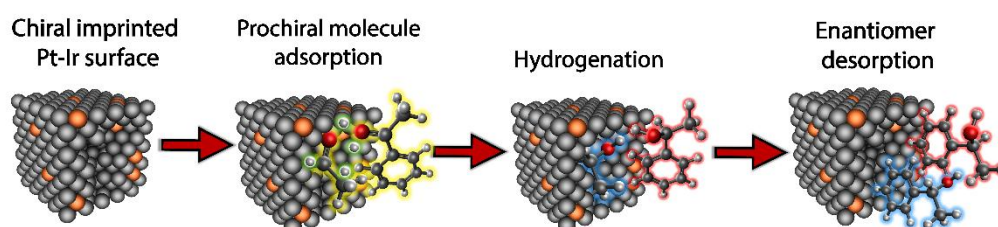
The asymmetric synthesis of PE enantiomers via the hydrogenation of ACE has been chosen in this proof-of-concept study as a simple model reaction to demonstrate for the first time the utility of chiral encoded Pt-Ir surfaces in heterogeneous catalysis. This carbonyl compound is generally found in bio-oil fractions,<sup>26</sup> and pure enantiomers of PE are significant chiral building blocks for pharmaceutical manufacturing to produce other high added-value products<sup>27</sup>. Although enantioselective electrosynthesis of phenylethanol has been previously achieved using chiral imprinted mesoporous Pt-Ir electrodes<sup>14d</sup>, the requirement of electrical energy and scale-up issues might be a concern. In order to overcome these potential limitations and to extend the scope of utilization of chiral imprinted metal surfaces to more traditional catalytic processes at low temperature, we have designed chiral imprinted Pt-Ir alloys supported on Ni foam for testing their application as heterogeneous catalysts for chiral synthesis. As illustrated in Scheme 2a, prochiral molecules are initially adsorbed at the enantioselective reaction sites and subsequently react with the hydrogen molecules present in the system. The hydrogenation process is selectively taking place under the influence of the local asymmetric environment to selectively produce chiral PE before the product is desorbed. Nevertheless, competing reactions at non-imprinted sites are unavoidable and mass transport limitations can slow down the evacuation of product, thus preventing the adsorption of fresh precursor molecules at the imprinted sites. This may lead to only modest enantioselectivity. In order to enhance the enantiomeric excess, a pulsed synthesis process, illustrated in Scheme 2b, in which product molecules are allowed to leave the surface during a certain waiting time without hydrogen supply, might be a promising alternative concept.

During conventional asymmetric synthesis, chiral PE is produced via selective hydrogenation of 1 mM acetophenone in an aqueous solution under static hydrogen atmosphere. Chiral products were analyzed at different reaction times using high-performance liquid chromatography (HPLC). The retention times of ACE, RPE and SPE are 9.6, 11.2 and 11.9 min, respectively, as can be seen in the corresponding chromatogram in Figure S9.

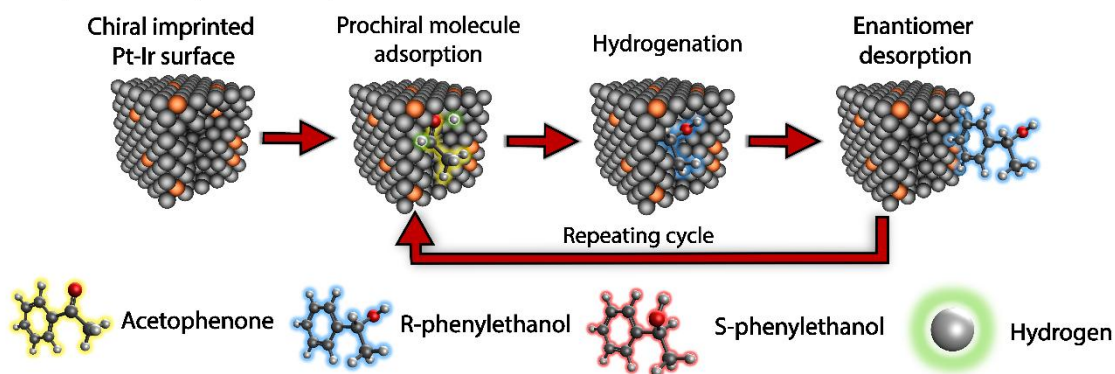
Several experimental parameters have an important influence on the final outcome of the synthesis. For example, the solution pH has a very significant effect on the catalytic performance, and a lower pH gives rise to a remarkable increase in enantiomeric excess from 49 to 80 %ee when decreasing the pH from 7 to 3 as illustrated in Figure S10 and Table S3. However, a too low pH (pH=1) results in a pronounced decrease in enantioselectivity (66 %ee) due to a too fast, and therefore unselective, reaction. The most suitable pH of the reaction medium is approximately 3, leading to a maximum enantiomeric excess. A control experiment carried out under the same conditions, but in the absence of chiral surface features with non-imprinted mesoporous Pt-Ir shows no significant enantiomeric excess (0.4 %ee). The error bar or the s.e.m. of the %ee values ( $\pm 0.6\%$ ), estimated by equation 2, confirms that without chiral features, there is no enantioselectivity. However, the Pt-Ir matrix imprinted with RPE exhibits a high %ee of  $80.2 \pm 2.7\%$  as mentioned above and shown in Figure 4a. When using a surface imprinted with SPE, the opposite scenario is observed with a preferential production of SPE as a desired product with  $78.4 \pm 3.1\%$  ee. In addition, the impact of reaction time on the degree of enantioselectivity was studied in more detail. As can be seen in Figure 4b, the enantioselectivity tends to decrease when prolonging the reaction time (79.6, 29.8 and 4.0% ee for 5, 10, and 15 min reaction time, respectively) and physical blocking of the chiral active sites by organic compounds might be the origin of this observation<sup>28</sup>. To better understand and eventually circumvent this passivation problem, the alloy has been used in a next set of experiments only for 5 min, followed by rinsing in water for 15 min, then immersed again in the same educt

solution for another 5 min, followed by 15 min rinsing and then dipped a last time in the already partially converted solution for 5 min. This corresponds, as before, to global reaction times of 5, 10 and 15 min, but interrupted by a cleaning step after every five minutes. Interestingly in this case the %ee measured after every step does not change, with an average value of 79.5%, irrespective of the global reaction time (see Figure S11 and Table S4). We can conclude that indeed a continuous prolonged exposure of the catalyst to the reaction medium leads to a blocking of the chiral sites, however this inhibition is reversible because full enantioselectivity can be recovered by simple rinsing in water.

### a) Conventional hydrogenation



### b) Pulsed asymmetric synthesis



Scheme 2. Chiral phenylethanol is synthesized from the prochiral starting compound, acetophenone, using: a) a conventional hydrogenation process and b) pulsed hydrogenation at chiral imprinted Pt-Ir alloy surfaces.

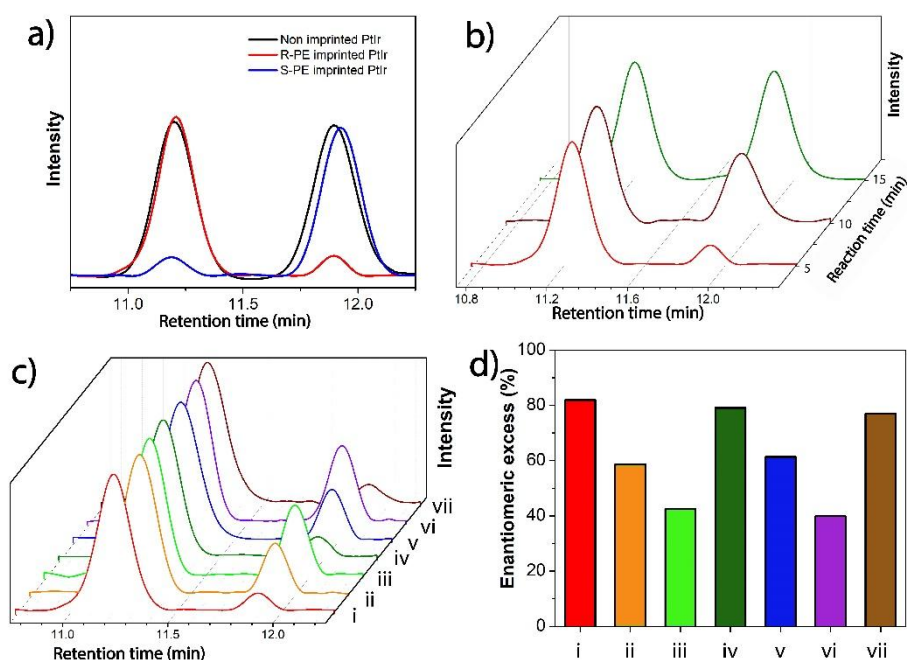


Figure 4 Analysis of reaction products from asymmetric hydrogenation of acetophenone: a) HPLC chromatograms of chiral products obtained by using chiral Pt-Ir alloy imprinted with RPE (red) and SPE (blue) as well as non-imprinted Pt-Ir (black); b) HPLC chromatograms of products obtained with RPE imprinted mesoporous Pt-Ir in 1 mM acetophenone for different reaction times using continuous conventional hydrogenation: 5 min (red), 10 min (brown), 15 min (green); c) and d) HPLC chromatograms of chiral products and histograms summarizing the enantiomeric excess (%ee) obtained with a chiral Pt-Ir alloy imprinted with RPE for three independent consecutive catalytic cycles in fresh educt solution for every cycle and rinsing in water after every full cycle: First catalytic cycle after a total reaction time of (i) 5 min (red), (ii) 7 min (orange), (iii) 9 min (light green); Second catalytic cycle after a total reaction time of (iv) 5 min (dark green), (v) 7 min (blue), (vi) 9 min (purple); (vii) Third catalytic cycle after a total reaction time of 5 min (brown).

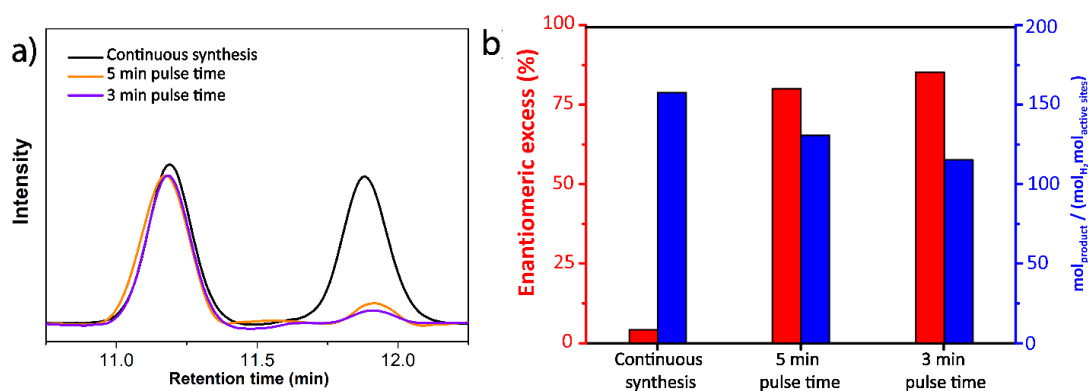


Figure 5. Pulsed asymmetric catalysis with chiral encoded Pt-Ir alloy supported on Ni foam a) HPLC chromatograms of products obtained with RPE imprinted mesoporous Pt-Ir in 1 mM acetophenone for continuous synthesis (black), pulsed asymmetric synthesis with a pulse time of 5 min (orange) and 3 min (purple).

3 min (purple) with a total synthesis time of 15 min. The retention times of 11.2 and 11.9 min correspond to RPE and SPE, respectively. b) Relationship between the enantiomeric excess and catalytic efficiency comparing conventional and pulsed synthesis.

In order to evaluate the global stability of the catalyst, the alloy has been used for several independent catalysis experiments, with intermittent rinsing in water only after every full catalytic cycle. For the first catalytic cycle, the enantioselectivity has been measured after different reaction times (5, 7, and 9 min), and decreases gradually from 82.0 to 58.6 and 42.5 %, respectively (Figure 4c and 4d). However, after rinsing in water and putting the catalyst again into a fresh educt solution for a second catalytic cycle, a high ee% of almost 80 % was again measured after a reaction time of 5 min. No significant decrease is observed for the same reaction time during a third cycle. This comparison of individual %ee values for a given reaction time (e.g. for cases I, IV and VII in Figure 6d for 5 min reaction time) illustrates the high stability and reusability of the chiral alloy. As reported previously, the stability of the imprinted Pt-Ir is remarkably improved compared to the monometallic Pt analog due to the presence of Ir atoms in the Pt bulk, positively influencing the local cohesion energy.<sup>14d</sup>

The enantiomeric excess can be optimized not only by using short reaction times as indicated above, but also by following a pulsed synthesis strategy (Scheme 2b). During a first step, the ketone educt is allowed to infiltrate the catalyst matrix in the absence of hydrogen. Once the prochiral precursor is adsorbed at the chiral reaction sites, hydrogen gas is flown into the reaction system for 5 min in order to generate the chiral PE product. Subsequently, the hydrogen flow is replaced by a stream of nitrogen for 15 min. During this relaxation period, the chiral product can desorb from the enantioselective sites, thus avoiding surface passivation (vide supra), and fresh precursor molecules can adsorb again at active sites for the next catalysis period in the presence of hydrogen. The hydrogen gas flow was switched on and off in several cycles to achieve high enantiomeric excess and an improved global yield. In a first set of experiments, a total catalytic reaction period of 15 min (3 times 5 min) has been chosen in order to compare with the previous experiments for which hydrogen has been flowing continuously for 15 min. A remarkable increase in %ee from 4% to 79.8% is observed, which can be further improved to up to 85 % when using an even shorter pulse time of 3 min (Figure 5).

The amount of product generated per unit of H<sub>2</sub> and catalyst is the second most important parameter in this type of experiments. With the current set-up, an overall catalytic efficiency, expressed by the amount of product with respect to amount of H<sub>2</sub> and catalyst (moleproduct/(moleH<sub>2</sub> moleactive sites)), in the range of 116 to 162 mol<sup>-1</sup> is obtained, depending on the experimental conditions (Figure 5b). Although the catalytic efficiency slightly decreases when using the pulsed synthesis strategy, compared to continuous operation, this loss is compensated by the considerably improved enantiomeric excess.

In order to further characterize the catalytic performance, %yield and enantiomeric excess are calculated and compared for conventional and pulse synthesis in Table S5. Hydrogenation of acetophenone on a chiral encoded bimetallic surface via a conventional procedure provides an average yield of 0.11% with only 4 %ee. Interestingly, when using pulsed conversion with short pulse durations of 5s and 3s, respectively, the %ee of phenylethanol is dramatically increasing to 80 and 85%, with a slightly decreased yield of 0.08 and 0.09%. Even though these values are rather low, they can be considered as a significant improvement with respect to results reported in the literature for acetophenone reduction on a cinchonine-doped Pd (CN@Pd) surface<sup>4c</sup>. A very low yield of chiral

product has been observed in this case, and in particular almost no ee% can be detected when the chiral template has been removed. Compared with the electroreduction of acetophenone using chiral imprinted bimetallic surfaces (Table S5),<sup>14d</sup> the %yield and %ee values obtained in the present work are quite similar. However, they could be achieved with much shorter reaction times, most likely due to the quasi 3D catalyst structure, ensuring an additional high active surface area. The overall yield might be further increased by optimizing the reactor design, for example via a flow-through set-up, which would allow an easy and continuous switching between a H<sub>2</sub> and N<sub>2</sub> gas flow. However, this was not the primary goal of this study. We most importantly illustrate that pulsed asymmetric synthesis allows achieving high enantiomeric excess in heterogeneous catalysis based on the use of the chiral imprinted metal structures, thus validating the concept as a promising alternative approach.

## Conclusion

We have developed chiral imprinted mesoporous Pt-Ir alloys supported on high surface area Ni foam, obtained by electrodeposition in the simultaneous presence of a molecular chiral template and a lyotropic liquid crystal phase. The synergy between the porous Ni-foam and the mesoporous alloy leads to a hybrid material with interesting features in terms of catalytic behaviour. The prepared material retains chiral information even after the removal of chiral templates as evidenced by Differential Pulse Voltammetry. Most importantly, the Ni foam supported chiral Pt-Ir can be used as a heterogeneous catalyst for the asymmetric synthesis of phenylethanol by hydrogenation of acetophenone as a model compound. The resulting preferential formation of one enantiomer is attributed to the presence of chiral recognition sites in the porous metal structure. By fine-tuning the reaction conditions, especially when using pulsed synthesis, an enantiomeric excess of around 85 %ee can be obtained, even when the material is employed for several successive catalytic cycles. This first example illustrates the catalytic performance of such a rather unconventional material and opens up interesting perspectives for the engineering of chiral surfaces for asymmetric synthesis of high added-value chemicals.

## Acknowledgements

We would like to thank Mr. Thassanant Atitthep for technical advice with characterization techniques and acknowledge a grant from Vidyasirimedhi Institute of Science and Technology (VISTEC). This work was supported by the bilateral PICS program of CNRS. C. W. thanks the Mid-Career Research Grant 2020 from National Research Council of Thailand (NRCT5-RSA63025-03) and the Program Management Unit for Human Resources & Institutional Development, Research and Innovation NXPO (B05F630118). In addition, this work has been partially supported by the National Nanotechnology Center (NANOTEC), NSTDA, Ministry of Science and Technology, Thailand, through the Research Network NANOTEC (RNN). The project has also been partially funded by the European Research Council (ERC) under the European Union's Horizon 2020 research and innovation program (grant agreement no 741251, ERC Advanced grant ELECTRA).

Keywords: Chiral imprinted on Ni foam • asymmetric synthesis • chiral encoded mesoporous alloy • heterogeneous catalyst • pulsed synthesis

[1] J. L. Bada, Origins of homochirality. *Nature* 1995, 374, 594-595.

[2] a) S. Dutta, A. J. Gellman, Enantiomer surface chemistry: conglomerate versus racemate formation on surfaces. *Chem. Soc. Rev.* 2017, 46, 7787-7839. b) A. J. Gellman, W. T. Tysoe, F. Zaera, Surface chemistry for enantioselective catalysis. *Catal. Lett.* 2014, 145, 220-232. c) T. Yasukawa, R. Masuda, S. Kobayashi, Development of heterogeneous catalyst systems for the continuous synthesis of chiral amines via asymmetric hydrogenation. *Nat. Catal.* 2019, 2, 1088-1092.

[3] a) C. Alexander, L. Davidson, W. Hayes, Imprinted polymers: artificial molecular recognition materials with applications in synthesis and catalysis. *Tetrahedron* 2003, 59, 2025-2057. b) C. Hao, R. Gao, Y. Li, L. Xu, M. Sun, C. Xu, H. Kuang, Chiral semiconductor nanoparticles for protein catalysis and profiling. *Angew. Chem. Int. Ed.* 2019, 58, 7371-7374.

[4] a) C. F. McFadden, P. S. Cremer, A. J. Gellman, Adsorption of chiral alcohol on "chiral" metal surfaces. *Langmuir* 1996, 12, 2483-2487. b) C. Wattanakit, Y. B. S. Côme, V. Lapeyre, P. A. Bopp, M. Heim, S. Yadnum, S. Nokbin, C. Warakulwit, J. Limtrakul, Kuhn, A. Enantioselective recognition at mesoporous chiral metal surfaces. *Nat Commun.* 2014, 5, 3325. c) L. Durán Pachón, I. Yosef, T. Z. Markus, R. Naaman, D. Avnir, G. Rothenberg, Chiral imprinting of palladium with cinchona alkaloids. *Nat. Chem.* 2009, 1, 160-164.

[5] A. Baiker, Reflections on chiral metal surfaces and their potential for catalysis. *Catal. Today* 2005, 100, 159-170.

[6] a) S. Alonso, G. Santiago, I. Cea-Rama, L. Fernandez-Lopez, C. Coscolín, J. Modregger, A. K. Ressmann, M. Martínez- Martínez, H. Marrero, R. Bargiela, M. Pita, J. L. Gonzalez-Alfonso, M. L. Briand, D. Rojo, C. Barbas, F. J. Plou, P. N. Golyshin, P. Shahgaldian, J. Sanz-Aparicio, V. Guallar, M. Ferrer, Genetically engineered proteins with two active sites for enhanced biocatalysis and synergistic chemo- and biocatalysis. *Nat. Catal.* 2019, 3, 319-328. b) C. K. Savile, J. M. Janey, E. C. Mundorff, J. C. Moore, S. Tam, W. R. Jarvis, J. C. Colbeck, A. Krebber, F. J. Fleitz, J. Brands, P. N. Devine, G. W. Huisman, G. Hughes, Biocatalytic asymmetric synthesis of chiral amines from ketones applied to sitagliptin manufacture. *Science* 2010, 329, 305. c) L. J. Hepworth, S. P. France, S. Hussain, P. Both, N. J. Turner, S. L. Flitsch, Enzyme cascades in whole cells for the synthesis of chiral cyclic amines. *ACS Catal.* 2017, 7, 2920-2925.

[7] M. T. Reetz, What are the Limitations of enzymes in synthetic organic chemistry? *Chem. Rec.* 2016, 16, 2449-2459.

[8] V. Humblot, M. O. Lorenzo, C. J. Baddeley, S. Haq, R. Raval, Local and global chirality at surfaces: succinic acid versus tartaric acid on Cu(110). *J. Am. Chem. Soc.* 2004, 126, 6460-6469.

[9] R. M. Hazen, D. S. Sholl, Chiral selection on inorganic crystalline surfaces. *Nat. Mater.* 2003, 2, 367-374.

[10] a) G. A. Attard, Electrochemical studies of enantioselectivity at chiral metal surfaces. *J. Phy. Chem. B* 2001, 105, 3158-3167. b) L. Yang, J. Liu, P. Sun, Y. Ma, Z. Huang, Chiral nanoparticles: chiral ligand-free, optically active nanoparticles inherently composed of chiral lattices at the atomic scale, *Small* 2020, 16, 2070134.

[11] a) J. A. Switzer, H. M. Kothari, P. Poizot, S. Nakanishi, E. W. Bohannon, Enantiospecific electrodeposition of a chiral catalyst. *Nature* 2003, 425, 490-493. b) T. Yutthalekha, C. Warakulwit, J. Limtrakul, A. Kuhn, Enantioselective recognition of DOPA by mesoporous platinum imprinted with mandelic acid. *Electroanalysis* 2015, 27, 2209-2213. c) C. Wattanakit, Chiral metals as electrodes. *Curr. Opin. Electrochem.* 2018, 7, 54-60. d) S. Assavapanumat, B. Gupta, G. Salinas, B. Goudeau, C.

- Wattanakit, A. Kuhn, Chiral platinum-polypyrrole hybrid films as efficient enantioselective actuators. *Chem. Commun.* 2019, 55, 10956-10959.
- [12] G. S. Attard, P. N. Bartlett, N. R. B. Coleman, J. M. Elliott, J. R. Owen, J. H. Wang, Mesoporous platinum films from lyotropic liquid crystalline phases. *Science* 1997, 278, 838-840.
- [13] S. Assavapanumat, T. Yutthalekha, P. Garrigue, B. Goudeau, V. Lapeyre, A. Perro, N. Sojic, C. Wattanakit, A. Kuhn, Potential-induced fine-tuning of the enantioaffinity of chiral metal phases. *Angew. Chem. Int. Ed. Engl.* 2019, 58, 3471-3475.
- [14] a) T. Yutthalekha, C. Wattanakit, V. Lapeyre, S. Nokbin, C. Warakulwit, J. Limtrakul, A. Kuhn, Asymmetric synthesis using chiral-encoded metal. *Nat. Commun.* 2016, 7, 12678. b) C. Wattanakit, T. Yutthalekha, S. Assavapanumat, V. Lapeyre, A. Kuhn, Pulsed electroconversion for highly selective enantiomer synthesis. *Nat. Commun.* 2017, 8, 2087. c) S. Assavapanumat, M. Ketkaew, A. Kuhn, C. Wattanakit, Synthesis, characterization, and electrochemical applications of chiral Imprinted mesoporous Ni surfaces. *J. Am. Chem. Soc.* 2019, 141, 18870-18876. d) S. Butcha, S. Assavapanumat, S. Ittisanronnachai, V. Lapeyre, C. Wattanakit, A. Kuhn, Nanoengineered chiral Pt-Ir alloys for high-performance enantioselective electrosynthesis. *Nat. Commun.* 2021, 12, 1314.
- [15] E. Gross, J. H. Liu, S. Alayoglu, M. A. Marcus, S. C. Fakra, F. D. Toste, G. A. Somorjai, Asymmetric catalysis at the mesoscale: gold nanoclusters embedded in chiral self-assembled monolayer as heterogeneous catalyst for asymmetric reactions. *J. Am. Chem. Soc.* 2013, 135, 3881-3886.
- [16] T. Yasukawa, H. Miyamura, S. Kobayashi, Chiral metal nanoparticle-catalyzed asymmetric C-C bond formation reactions. *Chem. Soc. Rev.* 2014, 43, 1450-1461.
- [17] T. J. Lawton, V. Pushkarev, D. Wei, F. R. Lucci, D. S. Sholl, A. J. Gellman, E. C. H. Sykes, Long range chiral imprinting of Cu(110) by tartaric acid. *J. Phys. Chem. C* 2013, 117, 22290-22297.
- [18] I. Yosef, R. Abu-Reziq, D. Avnir, Entrapment of an organometallic complex within a metal: a concept for heterogeneous catalysis. *J. Am. Chem. Soc.* 2008, 130, 11880-11882.
- [19] C. Wattanakit, A. Kuhn, Encoding chiral molecular information in metal structures. *Chem. Eur. J.* 2020, 26, 2993-3003.
- [20] S. D. Lin, D. K. Sanders, M. Albert Vannice, Influence of metal-support effects on acetophenone hydrogenation over platinum. *Appl. Catal. A-Gen.* 1994, 113, 59-73.
- [21] J. A. Lopez-Ruiz, E. Andrews, S. A. Akhade, M. S. Lee, K. Koh, U. Sanyal, S. F. Yuk, A. J. Karkamkar, M. A. Derewinski, J. Holladay, V. A. Glezakou, R. Rousseau, O. Y. Gutiérrez, J. D. Hollday, Understanding the role of metal and molecular structure on the electrocatalytic hydrogenation of oxygenated organic compounds. *ACS Catal.* 2019, 9, 9964-9972.
- [22] S. Assavapanumat, M. Ketkaew, P. Garrigue, V. Lapeyre, S. Reculosa, C. Wattanakit, A. Kuhn, Hierarchical multiporous nickel for oxygen evolution reaction in alkaline media. *ChemCatChem* 2019, 11, 5834-5834.
- [23] S. I. Dorovskikh, E. S. Vikulova, D. B. Kal'nyi, Y. V. Shubin, I. P. Asanov, E. A. Maximovskiy, A. K. Gurakovskii, N. B. Morozova, T. V. Basova, Bimetallic Pt,Ir-containing coatings formed by MOCVD for medical applications. *J. Mater. Sci. Mater. Med.* 2019, 30, 69.
- [24] a) F. Ramírez-Crescencio, R. Redón, A. Herrera-Gomez, G. Gomez-Sosa, M. Bravo-Sanchez, A. L. Fernandez-Osorio, Facile obtaining of iridium(0), platinum(0) and platinum(0)-iridium(0) alloy nanoparticles and the catalytic reduction of 4-nitrophenol. *Mat. Chem. Phys.* 2017, 201, 289-296. b)

T. T. Huynh, N. N. Dang, H. Q. Pham, Bimetallic PtIr nanoalloy on TiO<sub>2</sub>-based solid solution oxide with enhanced oxygen reduction and ethanol electro-oxidation performance in direct ethanol fuel cells. *Catal. Sci. Technol.* 2021, 11, 1571-1579.

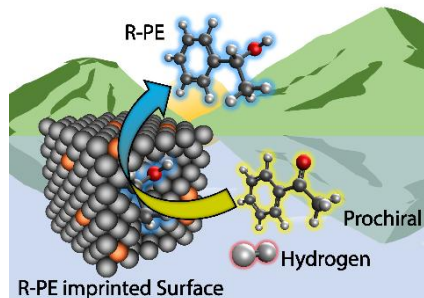
[25] E. N. E. Sawy, H. M. Molero, V. I. Birss, Methanol oxidation at porous co-electrodeposited Pt-Ir thin films. *Electrochim. Acta* 2014, 117, 202-210.

[26] A. P. P. Pires, J. Arauzo, I. Fonts, M. E. Domine, A. F. Arroyo, M. E. Garcia-Perez, J. Montoya, F. Chejne, P. Pfromm, M. Garcia-Perez, Challenges and opportunities for bio-oil refining: a review. *Energ. Fuel.* 2019, 33, 4683-4720.

[27] D. Mohan, C. U. Pittman, P. H. Steele, Pyrolysis of wood/biomass for bio-oil: a critical review. *Energ. Fuel.* 2006, 20, 848-889.

[28] M. D. Argyle, C. H. Bartholomew, Heterogeneous catalyst deactivation and regeneration: a review. *Catalysts* 2015, 5, 145-269.

Entry for the Table of Contents



Chiral imprinted mesoporous Pt-Ir supported on Ni foam was used to synthesize chiral compounds based on a heterogeneous catalysis approach. Fine-tuning the experimental conditions allows achieving high enantiomeric excess of one stereoisomer.

S. Assavapanumat, S. Butcha, S. Ittisanronnachai, A. Kuhn, C. Wattanakit\*